Downloaded from https://www.lyellcollection.org by volkan karabacak on Apr 27, 2023

JGS
Journal of the Geological Society

Perspective

https://doi.org/10.1144/jgs2023-020 | Vol. 180 | 2023 | jgs2023-020

The 2023 Pazarcık (Kahramanmaraş, Türkiye) earthquake (M_w 7.7): implications for surface rupture dynamics along the East Anatolian Fault Zone

Volkan Karabacak[1]*, Çağlar Özkaymak[2,3], Hasan Sözbilir[4,5], Orhan Tatar[6], Bahadır Aktuğ[7], Özkan Cevdet Özdağ[5], Recep Çakir[6], Ercan Aksoy[8], Fikret Koçbulut[9], Mustafa Softa[4], Elif Akgün[8], Ahmet Demir[6] and Gökhan Arslan[6]

[1] Department of Geological Engineering, Eskisehir Osmangazi University, 26040 Eskisehir, Türkiye
[2] Earthquake Implementation and Research Center, Afyon Kocatepe University, 03200 Afyonkarahisar, Türkiye
[3] Department of Geological Engineering, Engineering Faculty, Afyon Kocatepe University, 03200 Afyonkarahisar, Türkiye
[4] Department of Geological Engineering, Engineering Faculty, Dokuz Eylül University, 35390 İzmir, Türkiye
[5] Earthquake Research and Implementation Center, Dokuz Eylül University, 35390 İzmir, Türkiye
[6] Disaster and Emergency Management Authority of Türkiye, 06800 Ankara, Türkiye
[7] Department of Geophysical Engineering, Engineering Faculty, Ankara University, 06830 Ankara, Türkiye
[8] Department of Geological Engineering, Fırat University, 23119 Elazığ, Türkiye
[9] Department of Geological Engineering, Sivas Cumhuriyet University, 58140 Sivas, Türkiye

VK, 0000-0003-2581-7984; ÇÖ, 0000-0002-0377-1324; BA, 0000-0002-7995-4477; EA, 0000-0001-5078-7217; FK, 0000-0003-3578-029X

* Correspondence: karabacak@ogu.edu.tr

Abstract: Southern Türkiye faced widespread catastrophic destruction by two devastating earthquakes on the same day. As the earthquakes occurred at 04:17 (M_w = 7.7, Pazarcık, Kahramanmaraş) and 12:30 (M_w = 7.6, Elbistan, Kahramanmaraş) on 6 February 2023, neighbouring active fault systems were broken in succession between the Hatay and Malatya provinces in the region. The first earthquake, one of the largest earthquakes in this region during the last century, caused major fatalities and widespread damage to infrastructure and buildings, and produced large-scale seismo-gravitational surface deformation such as landslides, lateral spreading, liquefaction and extensional cracks. Here, we present the surface rupture geometry and coseismic displacement characteristics of the fault systems, determined by field observations immediately after the 6 February 2023 Pazarcık (Kahramanmaraş, Türkiye) earthquake (M_w = 7.7). Preliminary results show that the total rupture length (L_{max}) is 270 ± 10 km on the Karasu, Pazarcık and Erkenek segments of the East Anatolian Fault Zone. Left-lateral strike-slip faulting developed with a maximum horizontal displacement (D_{max}) of 7.30 m and an average displacement (D_{avg}) of 3.00 m. Although the surface rupture generally exhibits a narrow deformation zone width of 2–5 m, this expands to 50 m in some sections of the faults. The implications for rupture dynamics suggest that fracture development started on a secondary fault (Narlı Fault), transferred to the main fault and triggered the breaking of asperities on the Pazarcık segment, which exhibits a long period of accumulation of stress, to initiate the major rupturing.

Supplementary material: Figures S1–S12 with details on coseismic displacement are available at https://doi.org/10.6084/m9.figshare.c.6487245

Received 24 February 2023; **revised** 23 March 2023; **accepted** 24 March 2023

The East Anatolian Fault Zone (EAFZ) is one of the most significant active tectonic structures of the Eastern Mediterranean region that takes up the left-lateral relative motion between the Anatolian and Arabian plates. Together with the North Anatolian Fault Zone (NAFZ), the EAFZ accommodates the westward extrusion of the Anatolian plate (Şengör *et al.* 1985; Tatar *et al.* 2004). The fault zone extends for about 550 km in length from the Karlıova triple junction to the Mediterranean Sea in a NE–SW direction (Fig. 1a). The EAFZ encounters the Bitlis–Zagros Suture Zone (BZSZ) in the central part of its length, near Çelikhan, and evolves into a complex geometry towards the west (Fig. 1b). The main fault runs through from the vicinity of Çelikhan to Türkoğlu in a SW direction. It makes a 20° anticlockwise turn near Türkoğlu and continues along the western slopes of the Karasu Valley to the Amik Basin in a SSW direction. The EAFZ intersects the northern segments of the Dead Sea Fault Zone (DSFZ) to the south in at least two discrete areas, one to the east of Türkoğlu and near the town of Narlı and the second farther south in the Amik Basin immediately to the north of the city of Hatay (and the ancient city of Antioch) (Fig. 1b).

In previous studies, the main continuation of the EAFZ between Çelikhan (to the NW of the city of Adıyaman) and the Amik Basin is generally divided into five segments on the basis of geometric characteristics (Karabacak 2007; Karabacak *et al.* 2012; Duman and Emre 2013) (Fig. 1b). According to historical earthquake catalogues, segments extending to Çelikhan in the NE were reactivated by a series of M_s > 7 earthquakes between 1866 and 1905, whereas the Pütürge segment of the fault farther to the east was last ruptured by the 2020 Elazığ earthquake (M_w = 6.8) (Fig. 1b). Additionally, earthquakes in 1114 (I_0: X), 1513 (I_0: VIII), 1822 (M_s = 7.5) and 1893 (M_s > 7) were attributed to the fault continuation between Çelikhan and the Amik Basin (Arvanitakis 1903; Sieberg 1932; Calvi 1941; Pınar and Lahn 1952; Ben-Manahem 1979; Soysal *et al.* 1981; Ambraseys 1989; Ambraseys and Jackson 1998; Guidoboni and Comastri 2005). Although evaluation of historical earthquakes (Ambraseys 1989) and Coulomb stress changes (Nalbant *et al.* 2002) along the EAFZ imply that the fault segment between Gölbaşı and Türkoğlu constitutes a seismic gap, the first palaeoseismological studies, conducted by Karabacak *et al.* (2012) and Yönlü (2012),

© 2023 The Author(s). Published by The Geological Society of London. All rights reserved. For permissions: http://www.geolsoc.org.uk/permissions. Publishing disclaimer: www.geolsoc.org.uk/pub_ethics

Downloaded from https://www.lyellcollection.org by volkan karabacak on Apr 27, 2023

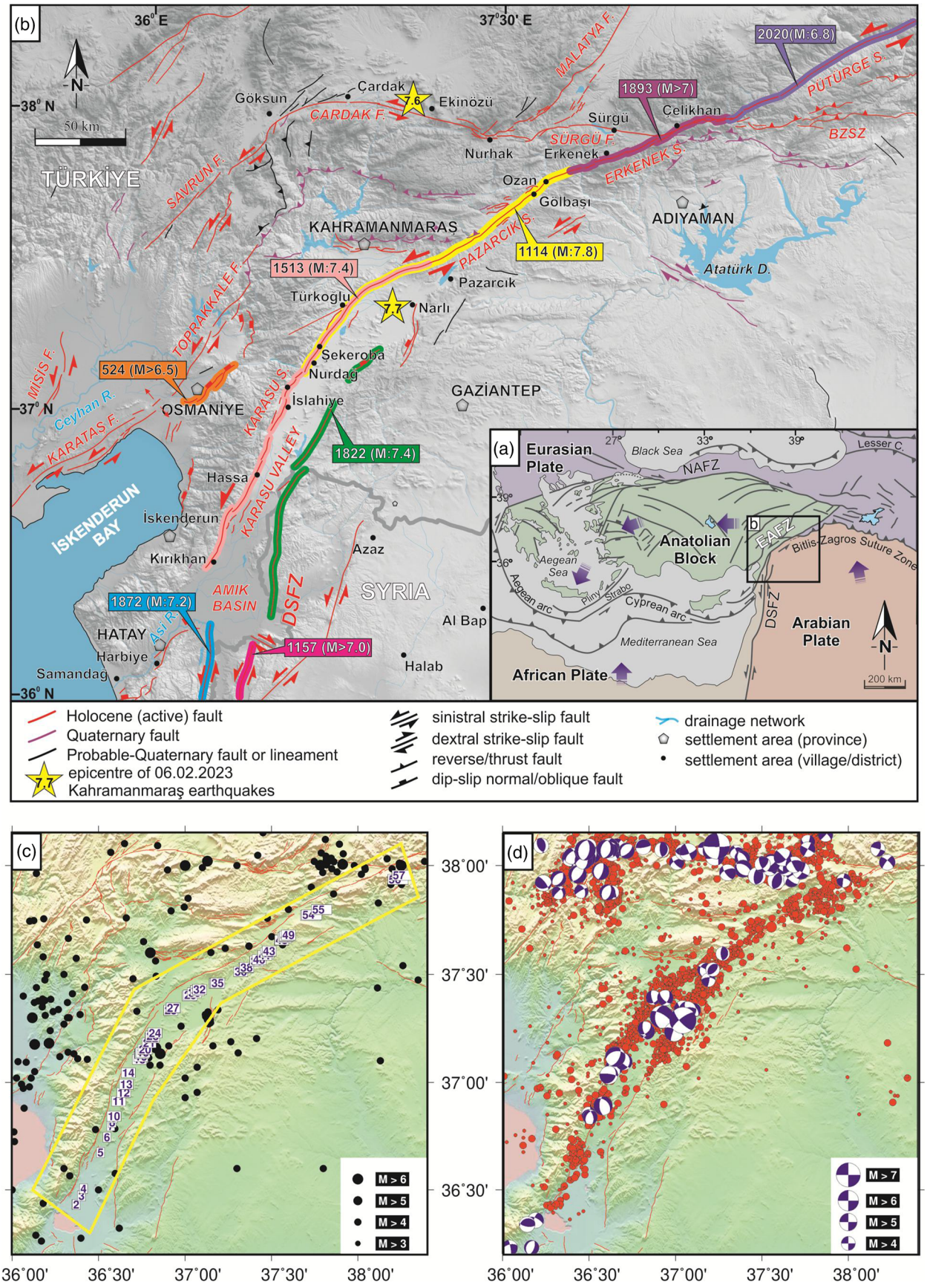


Fig. 1. (**a**) Tectonic outline of the eastern Mediterranean area and the location of the East Anatolian Fault Zone (EAFZ) between the Eurasian, African, Arabian and Anatolian blocks. DSFZ, Dead Sea Fault Zone; NAFZ, North Anatolian Fault Zone; Lesser C., Lesser Caucasus. Base map was generated using SRTM Plus V3 digital data. (**b**) Geometric fault segments of the East Anatolian Fault Zone (EAFZ) between the Bitlis–Zagros Suture Zone (BZSZ) and Amik Basin and historical earthquake activities along these segments. (**c**) Seismicity in the region before 6 February. The yellow outline defines the area where the aftershocks are projected along the fault. Observation points are shown by blue numbers. (**d**) Distribution of aftershocks and the focal mechanism solutions. Sources: (a) compiled from Özkaymak 2015; (b) palaeoseismological results from Karabacak (2007), Karabacak *et al.* (2012) and Yönlü *et al.* (2012, 2017); earthquake catalogues from Arvanitakis (1903), Sieberg (1932), Calvi (1941), Pınar and Lahn (1952), Ben-Manahem (1979), Soysal *et al.* (1981), Ambraseys (1989), Ambraseys and Jackson (1998) and Guidoboni and Comastri (2005); (c) earthquake catalogue from Kartal *et al.* (2022); (d) AFAD (2023).

Downloaded from https://www.lyellcollection.org by volkan karabacak on Apr 27, 2023

provided a unique opportunity to understand the greatest seismic hazard risk along the southwestern part of the EAFZ after hundreds of years of quiescence. However, considering the large ($M_s > 7$) historical earthquakes and Global Navigation Satellite Systems (GNSS)-derived slip-rate calculations of 10.5 ± 0.6 mm a^{-1} (Aktuğ *et al.* 2016), the pre-event seismicity in the region has been minimal (Fig. 1c).

The section of the EAFZ located between Çelikhan and the Amik Basin ended its silence on 6 February 2023 with an earthquake at 04:17 local time and having an instrumental moment magnitude (M_w) of 7.7. The epicentre of this earthquake was located near Pazarcık (Kahramanmaraş) (Fig. 1d). The earthquake, which took place at a depth of *c.* 8.6 km at 37.236°N, 37.057°E (Disaster and Emergency Management Authority of Türkiye – Earthquake Department (AFAD–DDB) records), resulted in a rupture exceeding 270 km (Fig. 2) and was closely followed by numerous aftershocks (*c.* 5500 aftershocks, the largest of which was $M_w = 6.7$, were recorded within the first 11 days after the main shock). It caused widespread infrastructure damage, at least 50 000 deaths (official count), and collapse or severe damage of about 212 000 buildings in 10 cities all located around the ruptured zone in southeastern Türkiye. We therefore carried out a field campaign along the earthquake surface rupture within the first 10 days after the main shock. The geometry and surface rupture characteristics, which correlated with orthophoto images, were analysed and mapped with a scale of 1:25 000 immediately after the earthquake. This paper presents our preliminary field observations regarding the length of the surface rupture of the Pazarcık (Kahramanmaraş, Türkiye) earthquake (M_w = 7.7) and its coseismic displacement characteristics.

Surface rupture characteristics

We have used the previous active fault maps in the vicinity of the study area (i.e. Karabacak *et al.* 2012; Yönlü 2012; Emre *et al.* 2013). The key locations for the field study were determined by Göktürk satellite images (using HGM Küre v4.2.98 software). We have mapped the surface rupture using digital elevation data at *c.* 29 m ground pixel resolution (Advanced Spaceborne Thermal Emission and Reflection Radiometer Global Digital Elevation Model (AsterG-DEM) V3 digital data). Most of the coseismic displacement measurements were collected in the field by tape measure, and all measurements by tape measure were supported by high-resolution maps of each location. To produce the maps, we used Real Time Kinematic drone (DJI Phantom 4 RTK) measurements that are accurate to within a few centimetres, without using ground control points. PIX4D software was used to process the obtained data. The measurements of the locations that could not be reached in the field study were completed by digitizing the orthophoto images (computer-generated images of aerial photographs) provided to the researchers by the unmanned aerial vehicle flights made by the General Directorate of Maps of Turkey immediately after the earthquake.

The Amik Basin, where the EAFZ and DSFZ intersect (Karabacak *et al.* 2010; Karabacak and Altunel 2013), rises gently to the NE and connects with the NNE–SSW-trending Karasu Valley, which is delineated by high topographic escarpments both to the west and the east. Our field observations in the Karasu Valley shortly after the Pazarcık earthquake showed that the surface rupture extends along the western margin of the valley in an en echelon geometry (Fig. 3 and Supplementary material Fig. S1). The fracture development starts in the Amik Basin, on the western coast of the former Amik Lake. A series of en echelon oblique faults emanate from the southern end of the basin (see the location in Fig. 2). The rupture does not display clear surface evidence in the basin and thus it has been mapped as probable in this section. Farther north, passing Kırıkhan, the fault strikes in a N30°E direction towards Karacagıl to the north, where it steps over to the left about 2 km (Fig. 3a). The maximum sinistral offset on roads varies from 1.40 to 2.20 m between Kırıkhan and Karaçağıl in a simple narrow deformation zone up to 2 m wide (Fig. 4a; Figs S2 and S3). No vertical displacements are observed. The trend of the rupture is N20°E to the west of Karaçağıl. Towards to the north, the rupture

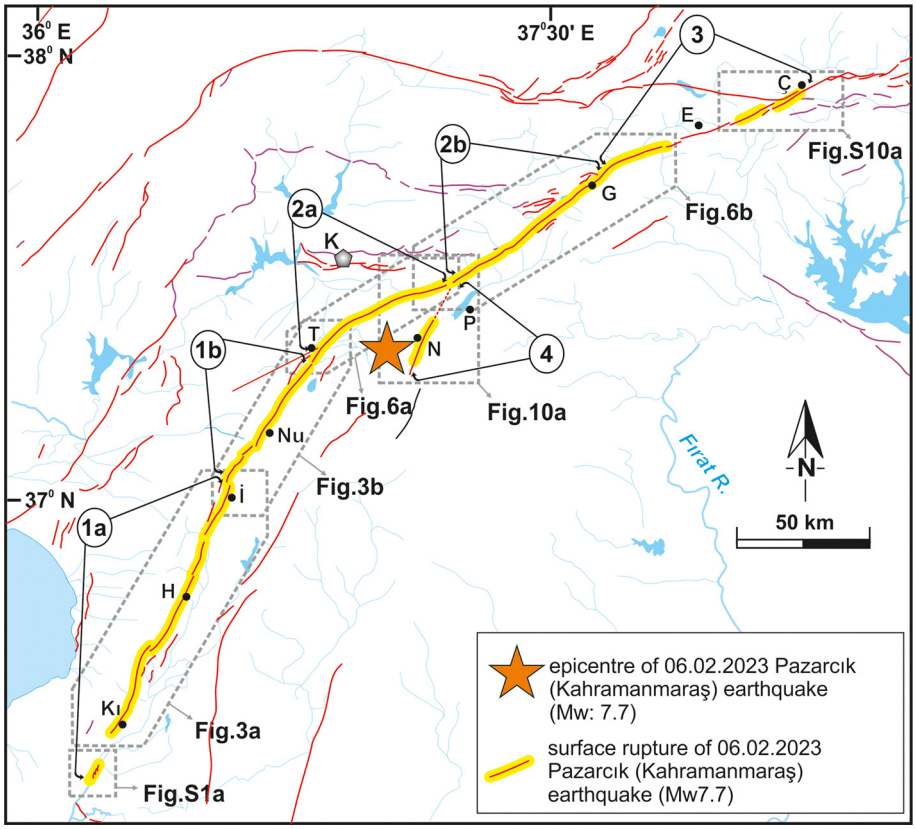


Fig. 2. Simplified map of the Pazarcık earthquake surface rupture and segmentations. 1a, Hassa rupture segment of the Karasu segment; 1b, Nurdağı rupture segment of the Karasu segment; 2a, Tevekkelli rupture segment of the Pazarcık segment; 2b, Gölbaşı rupture segment of the Pazarcık segment; 3, Erkenek segment; 4, Narlı Fault. K, Kahramanmaraş; Kı, Kırıkhan; H, Hassa; İ, İslahiye; Nu, Nurdağ; T, Türkoğlu; G, Gölbaşı; E, Erkenek; Ç, Çelikhan; P, Pazarcık; N, Narlı. Symbols are as in Figure 1.

Downloaded from https://www.lyellcollection.org by volkan karabacak on Apr 27, 2023

strikes in a N10°E direction to the south of Bektaşlı village, where a restraining bend is evident along the fault trace (Fig. 3a). Around the bend, in addition to left-lateral displacements of up to 2.00 m, vertical displacements of up to 0.50 m are also observed and measured. Farther north of Bektaşlı, the fault trends N30°E between Hassa and İslahiye (Fig. S4). Up to 4.50 m left-lateral displacement just south of Altınüzüm town indicates the maximum left-lateral motion on this strand (Hassa rupture segment of the Karasu segment; Fig. 3a).

The surface rupture steps over to the left for about 3 km around İslahiye (Fig. 3a), then it extends north towards Fevzipaşa, where the fault zone becomes nearly 50 m in width in a N30°E direction (Fig. 4b). Farther north, the rupture passes through Nurdağı and Şekeroba towns (Fig. 3b). Displacements varying from 1.60 to 3.80 m are measured on the roads, pavements, fences and railroad tracks (Fig. 5) on this strand of the fault (Nurdağı rupture segment of the Karasu segment). Leaving the western slope of the Amanos Mountain at Şekeroba, the surface rupture of the Karasu segment

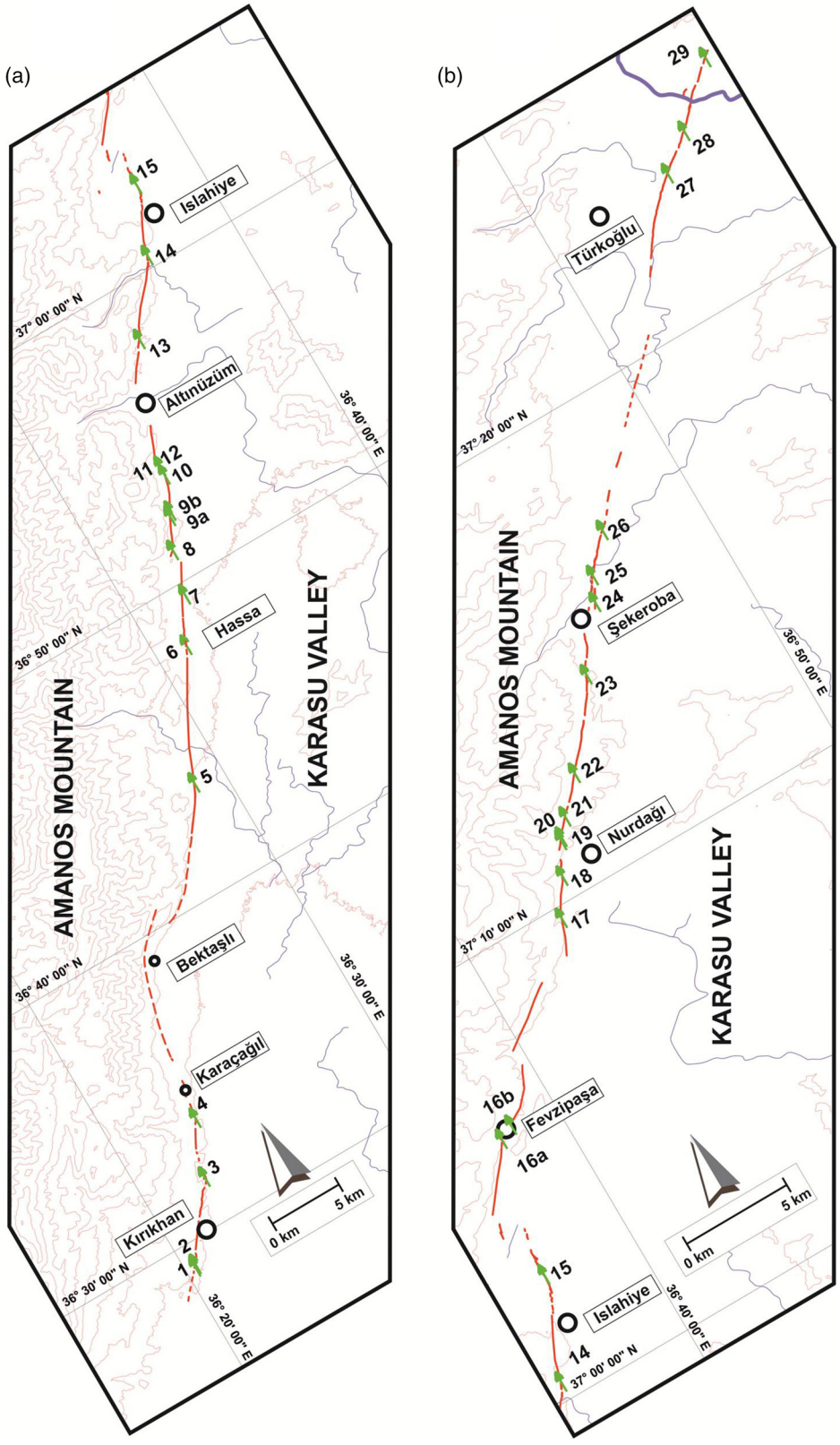


Fig. 3. Rupture geometry of the Pazarcık (Kahramanmaraş) earthquake along the Karasu segment of the EAFZ and slip distribution locations. (**a**) Hassa rupture segment; (**b**) Nurdağı rupture segment. Base maps were generated using AsterG-DEM V3 digital data.

Downloaded from https://www.lyellcollection.org by volkan karabacak on Apr 27, 2023

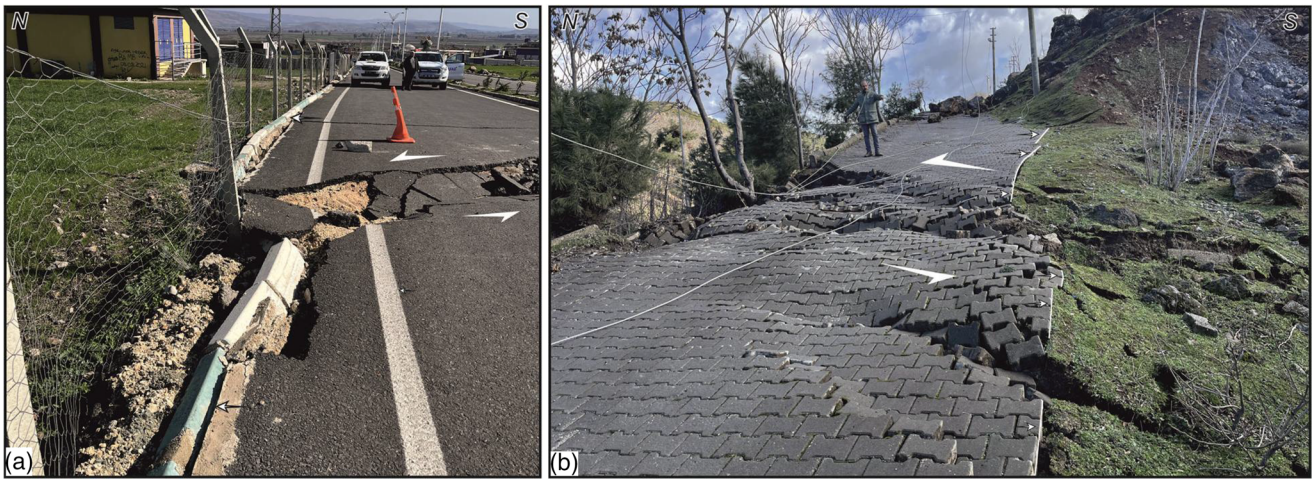


Fig. 4. Left-lateral displacements on the roads around (**a**) Kırıkhan (location 3; cars were used for scale) and (**b**) Fevzipaşa (location 16; a man about 1.8 m tall was used for scale).

descends to the Karasu valley floor and reaches to the east of Türkoğlu village. According to our detailed mapping, the surface rupture steps over to the left for about 1 km close to 37°20'00"N latitude (Fig. 3b). It crosscuts the Aksu River within the alluvial plain near Türkoğlu and reaches Kuyumcular village by making a 20° bend (Fig. S5). As it separates from the Karasu Valley in this area, the extent of the surface rupture changes and its strike turns to N45°E (Fig. 6a).

The surface rupture follows the contact between basement rocks and Quaternary alluvium deposits between Kocalar and Çiğli towns and follows the SE-facing long escarpment against the western edge of the Narlı Basin (Fig. 6a). Left-lateral offset stream channels in Plio-Quaternary sediments are an indicator of the recent activity along the fault. Near Kocalar village a cumulative offset of 1.3 km and sinistral displacements of up to 4.00 m are visible along field borders. Cropping out in a rather narrow zone near Tevekkelli (close to 37°00'00"E longitude in Fig. 6a) and Kapıçam (Fig. 7), the surface rupture extending to the east reaches Çiğli by displacing the Kahramanmaraş–Gaziantep highway left-laterally by 4.50 m (Fig. 8; Figs S6 and S7). There is no significant vertical displacement along this strand of the fault (Tevekkelli rupture segment of the Pazarcık segment), although left-lateral displacements ranging from 3.00 to 4.50 m are measured. Farther NE, the surface rupture continues into a mountainous area, and it makes a 1.5 km wide right bend near Kartal village (Fig. 6a), creating a local transpressional zone and causing local uplift owing to the presence of a contractional bend. Towards the NE, near Nacar village, the surface fault rupture exhibits a left step around the intersection area with the Narlı Fault lineament (Fig. 6a).

The measured coseismic displacements present a dramatic change (from *c.* 4 to *c.* 7 m) on the Pazarcık segment from the intersection area of the Narlı Fault lineament (Fig. 6b). This strand offers the clearest maximum displacement measurements. Displacements reach 7.30 m at the road and field boundaries farther east in the village of Nacar (Fig. S8). This follows the cumulative offsets at major streams (between 4.4 and 6.4 km) up to Sakarya village. Before entering the Gölbaşı Basin, coseismic displacements drop to 4.00 m again.

Field observations provided no evidence for surface faulting along the northern side of the Gölbaşı Basin (Fig. 6b). Therefore, our observations concentrated along the southern margin of the basin where the surface rupture limits the slopes to the south of the basin with a simple geometry. The maximum displacement measured along the rupture (Gölbaşı rupture segment of the Pazarcık segment) west of Balkar village reaches 6.00 m. The rupture reaches the Gölbaşı District farther east, in an ENE direction, passing through the village of Balkar (Figs 6b and 9; Fig. S9). The

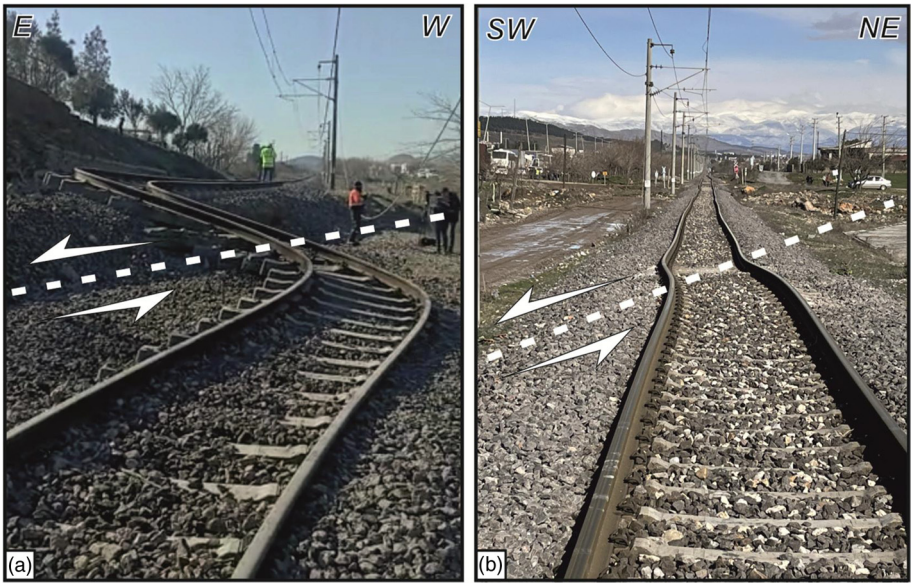


Fig. 5. Left-lateral displacements on the railways around Şekeroba (locations 24 and 25) (track gauge for the railway, which is used for scale, is 1.435 m).

Downloaded from https://www.lyellcollection.org by volkan karabacak on Apr 27, 2023

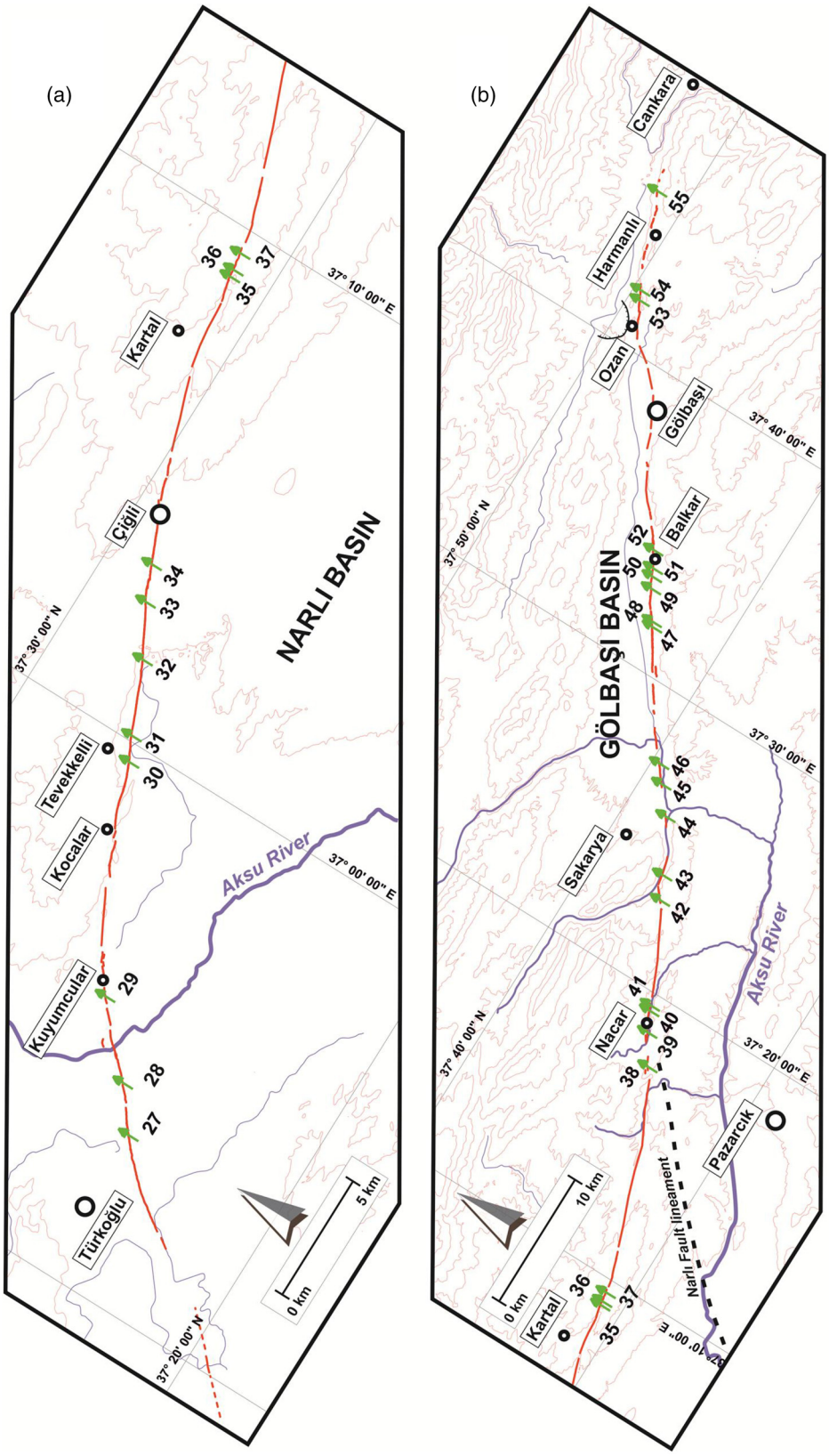


Fig. 6. Rupture geometry of the Pazarcık (Kahramanmaraş) earthquake along the Pazarcık segment of the EAFZ and slip distribution locations. (**a**) Tevekkelli rupture segment; (**b**) Gölbaşı rupture segment. Base maps were generated using AsterG-DEM V3 digital data.

surface rupture is not clear around Gölbaşı because of extensive liquefaction in the basin and numerous fault-parallel lateral spreading fractures.

The eastern end of the strand is well exposed to the NE of the Gölbaşı segment (Fig. 6b). This segment bends slightly to the left where it leaves the Gölbaşı Basin around Ozan village. The displacements decrease to 0.50 m on the fracture, progressing along the Erkenek segment in an ENE direction from the village of Ozan. Further east, near the village of Cankara (Fig. 6b), the rupture terminates by decreasing before reaching Cankara.

No surface rupture is observed for *c.* 30 km in the direction of Kurucaova (Fig. 2). However, just SE of Kurucaova, towards Balıkburnu and Çelikhan, the surface rupture is visible again (Fig. S10). In this area, it can be easily followed on a *c.* 10 km long

Downloaded from https://www.lyellcollection.org by volkan karabacak on Apr 27, 2023

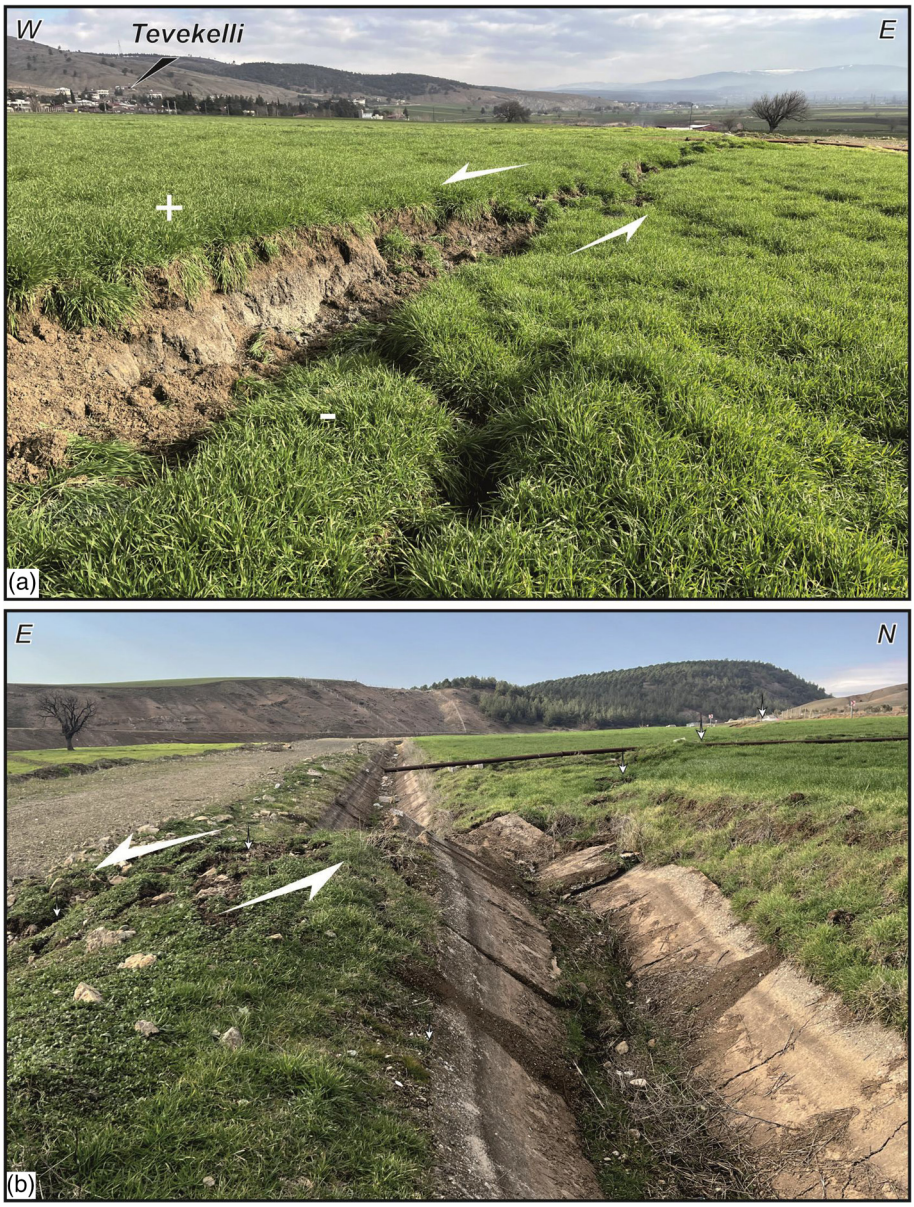


Fig. 7. (**a**) Vertical displacement (*c.* 0.35 m) in a field and (**b**) left-lateral displacements on a 1.6 m wide canal around Tevekkelli (location 31).

fracture in a N50E direction. The surface rupture ends south of Çelikhan.

Table 1 presents the entire displacement data along the Karasu, Pazarcık and Erkenek segments with co-ordinated surface rupture records. The Pazarcık earthquake also triggered a modest surface rupture (up to 10 km) on the northernmost tip of the DSFZ (Narlı Fault) extending towards the earthquake epicentre, which finalized lateral spreading in the Narlı Basin (Fig. 10a–c). The fault shows predominantly oblique normal fault morphology where the western block moves downward and the maximum vertical displacement on the fault is up to 1.60 m in the southernmost parts (Fig. 10d). The vertical displacement decreases towards the north and dominantly left-lateral displacements of up to 3.20 m are also observed (Fig. 10e and f). No surface rupture continues further NE of Bölükçam (Fig. 10a). However, just NE of Bölükçam, a 15 km long morphological lineament extends towards Nacar village. It is noteworthy that the coseismic displacements show an abrupt decrease on the Pazarcık segment from this intersection area towards the west (from *c.* 7 to *c.* 4 m).

In addition to the seismo-tectonic features, the main shock also caused large-scale seismo-gravitational surface deformation, such as landslides, lateral spreading, liquefaction and extensional cracks between Erkenek (Malatya) and Harbiye–Altınözü (Hatay) (Fig. 11).

Discussion

Slip distribution and surface observations indicate that a surface rupture occurred over 270 km during the Pazarcık (Kahramanmaraş) earthquake (M_w 7.7) along the southwestern continuation of the EAFZ between the Amik Basin and Çelikhan. The surface rupture developed on the Karasu, Pazarcık and partly on the Erkenek segments of the EAFZ. In the central part of the Erkenek segment, where the 1893 earthquake is attributed in historical earthquake catalogues, there is a 30 km gap without surface rupture or where it is unobserved under heavy snow cover.

Displacement measurements mapped along the surface rupture revealed that the displacement distribution was not symmetrical (Fig. 12). Accordingly, the maximum left-lateral displacement was measured as 7.30 m on the Pazarcık segment in the NE. A nearly 25 km long central section of the Pazarcık segment exhibits a displacement over 5 m. On average, 50% of displacement (from 2 to 4 m) occurs over 50% of the total length of the surface rupture (Fig. 12). On the Karasu segment, the maximum left-lateral displacement was measured as 4.50 m, whereas displacements vary from 1.40 to 2.20 m between Kırıkhan and Karaçağıl and from 1.60 to 3.80 m between the Nurdağı and Şekeroba segments (Fig. 12).

Downloaded from https://www.lyellcollection.org by volkan karabacak on Apr 27, 2023



Fig. 8. (**a**) Surface rupture in a field (electricity pylons (*c.* 20 m high) were used as scale) and (**b**, **c**) left-lateral displacements on Kahramanmaraş–Gaziantep highway (location 33; cars were used as scale).



Fig. 9. Surface rupture deformations and coseismic displacements from Balkar. (**a**) High-resolution map produced with an RTK drone and (**b**) field photograph of the left-lateral displacements on a road (location 51); (**c**, **d**) left-lateral displacements in the village (buildings used as scale have floor heights of about 3 m).

Downloaded from https://www.lyellcollection.org by volkan karabacak on Apr 27, 2023

Table 1. *Surface rupture characteristics of the Pazarcık earthquake (from SW to NE)*

Location	Coordinates (UTM)		Displacements (cm)		Width of ruptured zone (m)	Offset structure	Method
	Easting	Northing	Lateral	Vertical			
1	261646.00	4041203.00	140 ± 20	0	50	Refuge + road	Orthophoto
2	261732.00	4041325.00	150 ± 20	?	?	Field border	Orthophoto
3	264574.00	4045810.00	220 ± 10	0 ± 10	50	Road + refuge	Field data
4	265824.00	4049352.00	220 ± 10	?	4	Road	Field (mta)
5	275131.00	4067816.00	220 ± 10	50 ± 10	5	Road	Field (mta)
6	278616.00	4075646.00	310 ± 10	0 ± 10	3	Pavement + road + canal	Field data
7	278677.00	4075733.00	240 ± 10	?	5	Road	Field data
8	280289.00	4080950.00	340 ± 10	?	5	Road + field border	Field data
9	281485.00	4083 283.00	270 ± 10	0 ± 10	6	Wall + field border	Field (mta)
10	282392.00	4085754.00	370 ± 10	90 ± 10	15	Canal	Field data
11	282346.00	4085529.00	445 ± 10	?	6	Front door	Field data
12	282440.00	4086373.00	450 ± 10	50 ± 10	?	Fence	Field (mta)
13	285058.00	4094046.00	230 ± 20	?	5	Wall	Orthophoto
14	287334.00	4097601.00	190 ± 10	0	5	Road + bridge abutment	Field data
15	289196.00	4102412.00	140 ± 20	30 ± 10	10	Wall	Field data
16	290464.00	4108611.00	150 ± 10	90 ± 10	440*	Road + pavement	Field data
17	296275.00	4115348.00	160 ± 10	10 ± 10	?	Road	Field (mta)
18	297069.00	4116873.00	250 ± 10	50 ± 10	?	Pavement	Field (mta)
19	297688.00	4118206.00	200 ± 20	?	?	Road	Orthophoto
20	297758.00	4118322.00	230 ± 10	0 ± 10	?	Road	Field (mta)
21	298242.00	4118976.00	320 ± 10	50 ± 10	?	Pavement	Field (mta)
22	299316.00	4120359.00	360 ± 10	50 ± 10	?	Road	Field (mta)
23	301466.00	4123702.00	280 ± 20	?	4	Road + field border	Field data
24	303046.00	4126155.00	>90 ± 10	30 ± 10	255†	Railway	Field data
25	303465.00	4127193.00	200 ± 30	30 ± 20	10	Railway + wall	Field data
26	304575.00	4128626.00	180 ± 10	80 ± 10	?	Road	Field (mta)
27	312990.00	4140228.00	330 ± 20	?	?	Field border	Orthophoto
28	314246.00	4141407.00	380 ± 20	?	3	Canal	Field data
29	314246.00	4141407.00	360 ± 20	?	?	Field border	Orthophoto
30	322564.00	4147369.00	320 ± 20	0	?	Field border	Orthophoto
31	323278.00	4147798.00	360 ± 20	0	?	Field border + canal	Orthophoto
32	325389.00	4148900.00	320 ± 10	40 ± 10	4	Road	Field data
33	326913.00	4149917.00	450 ± 10	0 ± 10	5	Refuge + highway	Field data
34	327967.00	4150446.00	380 ± 20	?	?	Canal + field border	Orthophoto
35	336506.00	4153480.00	200 ± 20	?	?	Field border	Orthophoto
36	336732.00	4153501.00	200 ± 20	?	?	Field border	Orthophoto
37	337259.00	4153606.00	250 ± 20	?	?	Field border	Orthophoto
38	349175.00	4159233.00	300 ± 20	?	?	Path	Orthophoto
39	350778.00	4160491.00	730 ± 20	120 ± 10	45	Tree line	Field data
40	351891.00	4161143.00	730 ± 20	?	4	Road + field border	Field data
41	352167.00	4161296.00	620 ± 20	?	?	Field border	Orthophoto
42	357433.00	4164477.00	400 ± 20	?	?	Path	Orthophoto
43	358700.00	4165257.00	400 ± 20	?	?	Field border	Orthophoto
44	361569.00	4167170.00	340 ± 20	?	2	Field border	Field data
45	362987.00	4168582.00	470 ± 20	?	?	Field border	Orthophoto
46	363900.00	4169451.00	500 ± 20	?	?	Field border	Orthophoto
47	370173.00	4174793.00	600 ± 20	?	?	Road + canal	Orthophoto
48	370425.00	4175008.00	560 ± 20	0 ± 10	3	Road	Field data
49	371953.00	4176232.00	490 ± 20	?	?	Field border	Orthophoto
50	372556.00	4176621.00	370 ± 20	?	?	Road	Orthophoto
51	372969.00	4176856.00	380 ± 10	0 ± 10	3	Road	Field data
52	373849.00	4177500.00	330 ± 20	?	2	Road + field border	Field data
53	385260.00	4187316.00	260 ± 20	?	?	Field border	Orthophoto
54	385764.00	4187648.00	160 ± 20	?	2	Road	Field data
55	390922.00	4190231.00	50 ± 20	?	?	Road	Orthophoto
56	429863.00	4205184.00	430 ± 20	120 ± 20	3	Field border	Field data
57	431928.00	4207261.00	320 ± 10	30 ± 10	2	Road	Field data
58‡	334985.00	4134608.00	70 ± 10	160 ± 10	2	Field border	Field data
59‡	335479.00	4136485.00	90 ± 10	20 ± 10	4	Field border	Field data
60‡	335846.00	4137923.00	270 ± 10	50 ± 10	2	Road + field border	Field data
61‡	336679.00	4141843.00	320 ± 10	20 ± 10	3	Field border	Field data
62‡	338165.00	4144208.00	100 ± 10	20 ± 10	3	Railway + field border	Field data

*Ruptured zone in step-over.
†Ruptured zone with parallel branches.
‡Field data along the Narlı Fault.
Field data: in this study, (mta) indicates reported displacements in the field (Kürçer *et al.* 2023).

Downloaded from https://www.lyellcollection.org by volkan karabacak on Apr 27, 2023

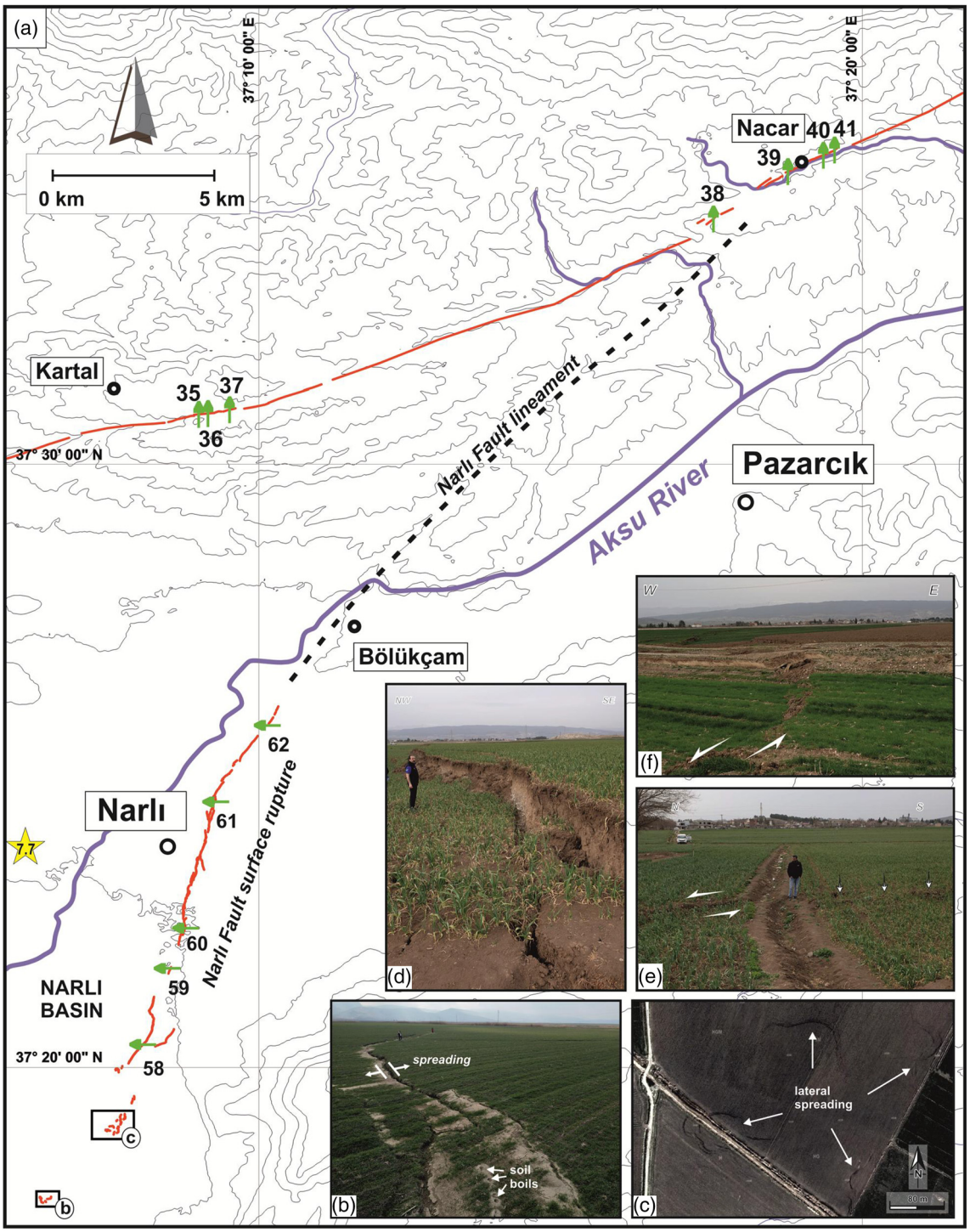


Fig. 10. (**a**) Rupture geometry of the Narlı Fault extending towards the earthquake epicentre and slip distribution locations. Base map was generated using AsterG-DEM V3 digital data. (**b**) Field photograph of the spreading and soil boils in the Narlı Basin (note that the dilatation along the fracture is about 0.30 m). (**c**) Orthophoto image of lateral spreading in the Narlı Basin. (**d**) Vertical displacement in a field (location 58; a man about 1.7 m tall was used for scale). (**e**) Left-lateral displacements on a field border (location 59; a man about 1.8 m tall was used for scale) and (**f**) railway around Narlı (location 62) (note the left lateral displacement of *c.* 1 m at the field boundary).

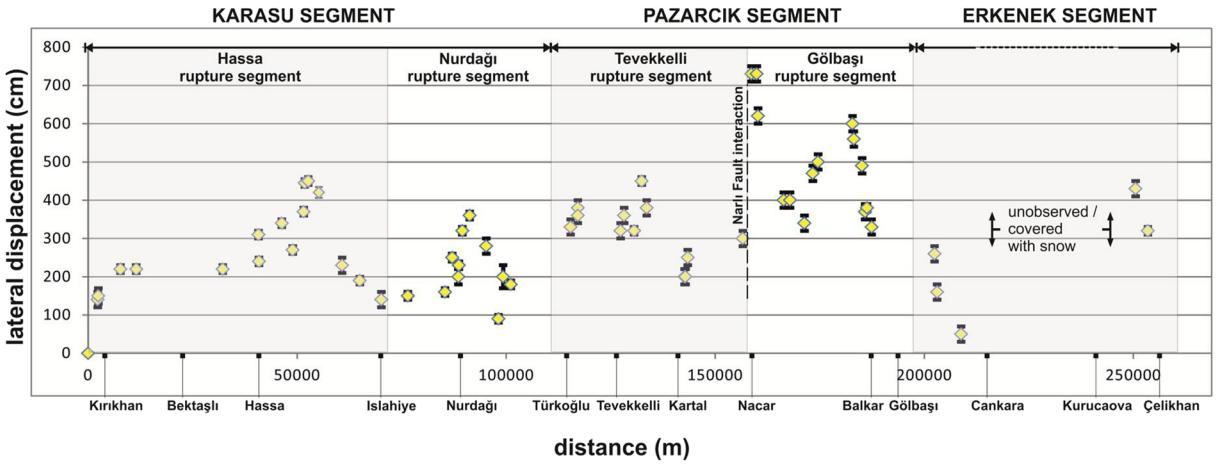
The locations of aftershocks located in the buffer zone outlined in yellow in Figure 1c were projected on the profile of rupture distance to correlate with the observed geological surface slips (Fig. 13). The aftershocks following the mainshock at 04:17 on 6 February are mostly concentrated in the middle part of the mapped surface rupture between İslahiye and Türkoğlu (Fig. 3). On the other hand, relatively lower surface slips are observed in this region, which is consistent with the fact that aftershocks localize near low-slip areas. The largest surface slips are observed between Nacar and Balkar (Fig. 13). The GNSS-derived slip deficit is about 5.35 ± 0.30 m, which corresponds to a confidence interval between 4.74 and 5.96 m at 95% confidence level. The highest slips observed are within the confidence limits of long-term strain accumulation. However, the southernmost part appears to be accumulating slip, with a low concentration of aftershocks and low surface slips.

The bending area of the main faults exhibits some complexity with multiscale faulting that may be expected generally be too small to produce a surface fault (King and Nabelek 1985). According to our detailed surface rupture mapping, the main fault makes a 20° bend near Türkoğlu (Fig. 2). Just east of the area of the bend, around

Downloaded from https://www.lyellcollection.org by volkan karabacak on Apr 27, 2023



Fig. 11. Seismo-gravitational deformation triggered by the earthquake around the study area. (**a**) Kocalar (between locations 30 and 31); (**b**) Döver (south of the Hatay); (**c**) Altınözü (Hatay) (note that the height of olive trees is about 2 m); (**d**) Demirköprü (south of Amik Basin).



left-lateral surface rupture displacement (D)(m)	cumulative length of the surface rupture (L) (km)
<2	58.2
2<D<3	69.2
3<D<4	57.6
4<D<5	16.0
5<D<6	5.1
6<D	3.2
D_{avg}: 3.00 m	
D_{max}: 7.30±0.20 m	L_{max}:270±10 km

Fig. 12. Distribution of left-lateral displacement along the surface rupture of the Pazarcık (Kahramanmaraş) earthquake.

Downloaded from https://www.lyellcollection.org by volkan karabacak on Apr 27, 2023

the Pazarcık epicentre ($M_w = 7.7$), a NNE-trending secondary surface rupture, the Narlı Fault, extends to the main fault. Aftershocks close to the Pazarcık epicentre are also distributed along two fault segments: the Pazarcık segment and the Narlı Fault (Fig. 1d). Because bending and multiple fault junction areas are the results of complex Earth crust architecture, a monotonous distribution of displacement along the earthquake surface rupture is not expected (King and Nabelek 1985; Klinger *et al.* 2006). Our results also support this situation. The measured coseismic displacements present a dramatic change in the Pazarcık segment from the intersection area of the Narlı Fault (Fig. 12).

Comparing the current surface rupture observations and coseismic displacement measurements of the Pazarcık earthquake with the historical earthquake records of previous studies (i.e. Karabacak *et al.* 2012; Yönlü *et al.* 2012) reveals the existence of two possible situations: (1) fracture development started along the Gölbaşı rupture segment where the displacement was at its maximum and mainly proceeded towards Türkoğlu in a SE direction, while it partly forced the northern end of the DSFZ (Narlı Fault) to extend towards the earthquake epicentre; (2) the bending areas in faults require a multiple fault junction of secondary faults, which may have a role in the breaking of asperities on the main fault plane to initiate the major earthquake (Aki 1979; King and Nabelek 1985; Klinger *et al.* 2006). The Pazarcık epicentre ($M_w = 7.7$) is fairly close to the NNE-trending Narlı Fault. Thus, fracture development started in the vicinity of Pazarcık near the epicentre but triggered and produced maximum displacement in the Gölbaşı rupture segment, which exhibits a long period of inactivity in the east and which has accumulated stress since the 1114 earthquake. Measured lateral displacements support the second possibility and the dramatic change in the Pazarcık segment from the intersection area could be interpreted in this way. The sum of the lateral displacements on the Tevekkelli rupture segment and on the Narlı Fault (*c.* 4 and *c.* 3 m, respectively) compensates for the displacement reaching 7 m along the Gölbaşı rupture segment, NE of Nacar.

The more southwesterly segments, which were previously broken during the 1513 earthquake, relieved a stress of about 500 years and revealed a lower amount of displacement. When evaluated with the prior geological slip rate estimations along the Karasu (*c.* 4–5 mm a^{-1}) and Pazarcık segments (*c.* 6–10 mm a^{-1}) (Karabacak 2007; Yönlü *et al.* 2017) it is striking that the accumulated stress and displacement amounts are consistent.

The observed vertical coseismic displacements are relatively low with respect to the lateral displacements, and this observation is consistent with the strike-slip regime of the region. Similarly,

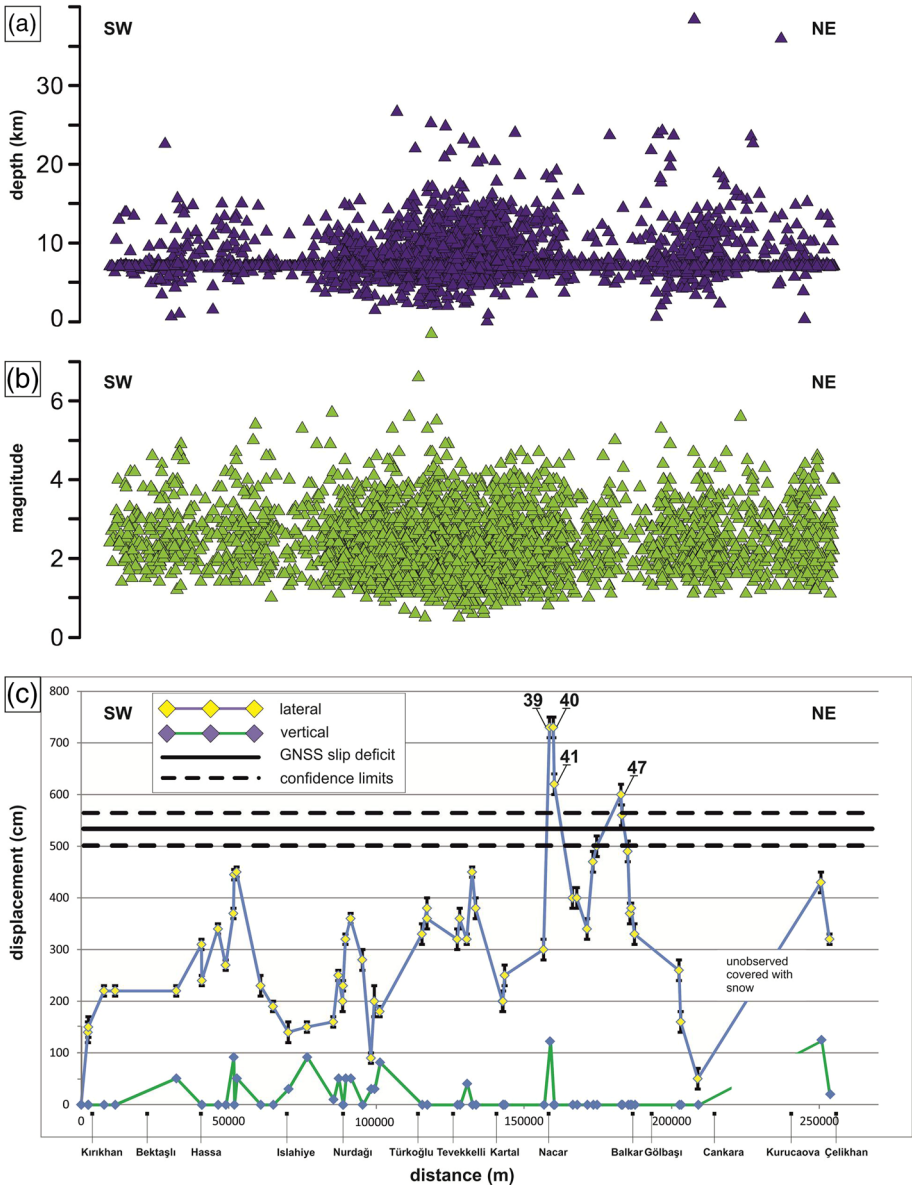


Fig. 13. Distribution of the earthquake depths (**a**), magnitudes (**b**), and lateral and vertical surface displacements along the surface rupture (**c**). The earthquakes within the zone outlined in yellow in Figure 1c were included in the analysis. The error bars of the observed displacements are given at 95% confidence level. Confidence limit of GNSS slip deficit is at 95% level.

Downloaded from https://www.lyellcollection.org by volkan karabacak on Apr 27, 2023

interseismic contraction rates between the Arabian and Anatolian plates were less than 3 mm a^{-1} whereas the left-lateral slip rates were 10.5 ± 0.6 mm a^{-1} (Aktuğ *et al.* 2016). Aktuğ *et al.* (2016) predicted the potential magnitude of an earthquake in this part of the region as M_w 7.7 by using a GNSS-derived slip rate of 10.5 mm a^{-1} and a time interval of 502 years since the 1513 earthquake. Considering the time elapsed (510 years) and slip rate of 10.5 ± 0.6 mm a^{-1}, a slip deficit of 5.35 ± 0.30 m is expected. Except for the southernmost part, the observed geological slips are close to the confidence bounds of the average slip deficit. In this respect, it is considered that the 6 February Pazarcık earthquakes released the strain energy accumulated since 1513. Considering the low recurrence rates of this segment, an earthquake of similar magnitude is not expected along these segments of the EAFZ in the near future.

Conclusions

(1) The 6 February 2023, M_w 7.7 Pazarcık (Kahramanmaraş, Türkiye) earthquake occurred along the southwestern continuation of the EAFZ as a result of the combined operation of three segments (Karasu, Pazarcık and Erkenek) and the Narlı Fault.

(2) Fracture development started in the vicinity of Pazarcık near the epicentre, transferred to the north via the Narlı Fault, triggered the breaking of asperities on the main fault (Pazarcık segment) to initiate the major rupturing, and produced maximum displacement in the Gölbaşı rupture segment, which exhibits a long period of accumulation of stress.

(3) The total surface rupture length (L_{max}) of the earthquake is 270 ± 10 km between the Amik Basin (Hatay) in the SW and Çelikhan (Adıyaman) in the NE.

(4) The surface rupture extends to the village of Cankara to the south of Erkenek in a NE direction. After a 30 km gap, it continues as a 10 km long surface rupture at the northernmost tip of the Erkenek segment. It terminates near Çelikhan near the intersection of the BZSZ, which obliquely cuts across the EAFZ farther north. To the south, the rupture development passes through Kırıkhan and ends in the Amik Basin. The surface rupture forced the northern end of the DSFZ in the Amik Basin and ended with a surface pattern of en echelon seismo-gravitational extensional surface deformations. Similar deformations were also observed in the Narlı Basin near the Narlı Fault, extending towards the earthquake epicentre.

(5) The average left-lateral displacement (D_{avg}) is about 3.00 m, whereas the maximum displacement (D_{max}) of the earthquake, measured on the Pazarcık segment, is 7.30 m.

(6) The concentration of aftershocks correlates with measured surface rupture displacements, and they cluster in the parts with low displacements.

(7) Taking elapsed time (500–900 years) and a slip rate of up to 10.5 mm a^{-1} into account, an average slip deficit over 5 m is expected, which is mostly consistent with observed surface slips.

Scientific editing by Yildirim Dilek

Acknowledgements We would like to thank the Disaster and Emergency Management Authority of Türkiye (AFAD) and the Scientific and Technological Research Council of Türkiye (TÜBİTAK) for their support in the field studies during this stressful period. We would also like to thank the General Directorate of Mapping of Türkiye (GDM) for providing high-quality orthophoto images to researchers immediately after the earthquake. Field assistance of A. Polat and B. Tekin (AFAD) is gratefully acknowledged. We are grateful to Y. Dilek, Journal Editor, for inviting this contribution. Appreciation is extended to two anonymous reviewers for their indispensable suggestions on the paper.

Author contributions **VK**: conceptualization (lead), formal analysis (lead), investigation (lead), methodology (lead), writing – original draft (lead), writing – review & editing (lead); **ÇÖ**: formal analysis (supporting), investigation (equal), methodology (equal), writing – review & editing (supporting); **HS**: formal analysis (supporting), investigation (equal), methodology (equal); **OT**: formal analysis (supporting), investigation (supporting), methodology (supporting); **BA**: formal analysis (supporting), investigation (supporting), writing – original draft (supporting); **ÖCÖ**: investigation (supporting); **RÇ**: investigation (supporting); **EA**: investigation (supporting); **FK**: investigation (supporting); **MS**: investigation (supporting); **EA**: investigation (supporting); **AD**: investigation (supporting); **GA**: investigation (supporting)

Funding This research received no specific grant from any funding agency in the public, commercial or not-for-profit sectors.

Competing interests The authors declare that they have no known competing financial interests or personal relationships that could have appeared to influence the work reported in this paper.

Data availability All data generated or analysed during this study are included in this published article and its Supplementary information files.

References

AFAD 2023. Presidency of Disaster and Emergency Management (AFAD), earthquake catalogue, https://deprem.afad.gov.tr/event-catalog [last accessed 19 February 2023].

Aki, K. 1979. Characterization of barriers on an earthquake fault. *Journal of Geophysical Research*, **84**, 6140–6148, https://doi.org/10.1029/jb084ib11p06140

Aktuğ, B., Özener, H. *et al.* 2016. Slip rates and seismic potential on the East Anatolian Fault System using an improved GPS velocity field. *Journal of Geodynamics*, **94–95**, 1–12, https://doi.org/10.1016/j.jog.2016.01.001

Ambraseys, N.N. 1989. Temporary seismic quiescence: SE Turkey. *Geophysical Journal International*, **96**, 311–331, https://doi.org/10.1111/j.1365-246X.1989.tb04453.x

Ambraseys, N.N. and Jackson, J.A. 1998. Faulting associated with historical and recent earthquakes in the Eastern Mediterranean region. *Geophysical Journal International*, **133**, 390–406, https://doi.org/10.1046/j.1365-246X.1998.00508.x

Arvanitakis, G.L. 1903. Essai d'une statistique des tremblements de terre en Palestine et Syrie. *Bulletin de l'Institut d'Égypte*, **4**, 178–183.

Ben-Manahem, A. 1979. Earthquake Catalogue for the Middle East (92 B.C.–1980 A.D.). *Bollettino di Geofisica Teorica ed Applicate*, **XXIN**, 81.

Calvi, W.S. 1941. *Erdbebenkatalog der Turkei und Einiger Benachbarter Gebiete*. MTA (General Directorate of Mineral Research and Exploration), Report **276**, Ankara [in German].

Duman, T.Y. and Emre, Ö. 2013. The East Anatolian Fault: geometry, segmentation, and jog characteristics. *Geological Society, London, Special Publications*, **372**, 495–529, https://doi.org/10.1144/SP372.14

Emre, Ö., Duman, T.Y., Özalp, S., Elmacı, H., Olgun, Ş. and Şaroğlu, F. 2013. *Active Fault Map of Turkey with an Explanatory Text 1:1,250,000 Scale*. General Directorate of Mineral Research and Exploration, Special Publication Series, **30**.

Guidoboni, E. and Comastri, A. 2005. *Catalogue of Earthquakes and Tsunamis in the Mediterranean Area from the 11th to the 15th Century*. Istituto Nazionale di Geofisica e Vulcanologia.

Karabacak, V. 2007. *Quaternary Activity of the Northern Dead Sea Fault Zone*. PhD thesis, Eskisehir Osmangazi University, Natural and Applied Sciences Institute [in Turkish with English abstract].

Karabacak, V. and Altunel, E. 2013. Evolution of the northern Dead Sea Fault Zone in southern Turkey. *Journal of Geodynamics*, **65**, 282–291, https://doi.org/10.1016/j.jog.2012.04.012

Karabacak, V., Altunel, E., Meghraoui, M. and Akyüz, H.S. 2010. Field evidences from northern Dead Sea Fault Zone (South Turkey): new findings for the initiation age and slip rate. *Tectonophysics*, **480**, 172–182, https://doi.org/10.1016/j.tecto.2009.10.001

Karabacak, V., Akyüz, H.S., Kıyak, N.G., Altunel, E., Meghraoui, M. and Yönlü, Ö. 2012. *The Late Quaternary Activity of the East Anatolian Fault Zone Between Gölbaşı (Adıyaman) and Karataş (Adana)*. TUBITAK (The Scientific & Technological Research Council of Turkey) Research Project, Final Report, Project No. **109Y043**.

Kartal, R.F., Kadirioğlu, F.T. and Kılıç, T. 2022. An improved earthquake and moment tensor catalogues ($M \geq 4.0$) for Anatolian region and its near vicinity (2013–2019). *Arabian Journal of Geosciences*, **15**, 1632, https://doi.org/10.1007/s12517-022-10933-6

King, G.C.P. and Nabelek, J. 1985. Role of fault bends in the initiation and termination of earthquake rupture. *Science*, **228**, 984–987, https://doi.org/10.1126/science.228.4702.984

Klinger, Y., Michel, R. and King, G.C.P. 2006. Evidence for an earthquake barrier model from Mw~7.8 Kokoxili (Tibet) earthquake slip-distribution. *Earth and Planetary Science Letters*, **242**, 354–364, https://doi.org/10.1016/j.epsl.2005.12.003

Downloaded from https://www.lyellcollection.org by volkan karabacak on Apr 27, 2023

Kürçer, A., Elmacı, H., Özdemir, E., Güven, C., Güler, T., Avcu, İ. and Özalp, S. 2023. *06 Şubat 2023 Pazarcık (Kahramanmaraş) Depremi (Mw 7,7) Saha Gözlem Raporları Serisi, 1 – Amanos Segmenti*. MTA (General Directorate of Mineral Research and Exploration), Report **14121**, Ankara [in Turkish].

Nalbant, S.S., McClusky, J., Steacy, S. and Barka, A. 2002. Stress accumulation and increased seismic risk in eastern Turkey. *Earth and Planetary Science Letters*, **195**, 291–298, https://doi.org/10.1016/S0012-821X(01)00592-1

Özkaymak, Ç. 2015. Tectonic analysis of the Honaz Fault (western Anatolia) using geomorphic indices and the regional implications. *Geodinamica Acta*, **27**, 110–129, https://doi.org/10.1080/09853111.2014.957504

Pınar, N. and Lahn, E. 1952. *Türkiye Depremleri İzahlı Kataloğu, Series 6*. Ministry of Construction and Settlement, Directorate of Construction and Zoning Affairs, Ankara.

Şengör, A.M.C., Görür, N. and Şaroğlu, F. 1985. Strike-slip deformation basin formation and sedimentation: strike-slip faulting and related basin formation in zones of tectonic escape: Turkey as a case study. *SEPM Special Publications*, **37**, 227–264, https://doi.org/10.2110/pec.85.37.0227

Sieberg, A. 1932. Erdbebengeographie. *In:* Gutenberg, B. (ed.) *Handbuch der Geophysik*, **4**. Borntraeger, Berlin, 775–812.

Soysal, H., Sipahioğlu, S., Kolçak, D. and Altınok, Y. 1981. *Earthquake catalogue of Turkey and surroundings, BC 2100–AD 1900*. TUBITAK (The Scientific & Technological Research Council of Turkey) Research Project, Final Report, **TBAG 341**.

Tatar, O., Piper, J.D.A., Gürsoy, H., Heimann, A. and Kocbulut, F. 2004. Neotectonic deformation in the transition zone between the Dead Sea Transform and the East Anatolian Fault Zone, Southern Turkey: a palaeomagnetic study of the Karasu Rift Volcanism. *Tectonophysics*, **385**, 17–43, https://doi.org/10.1016/j.tecto.2004.04.005

Yönlü, Ö. 2012. *The Late Quaternary Activity of Southwestern Part of the East Anatolian Fault Zone in Turkey*. PhD thesis, Eskişehir Osmangazi University, Eskişehir.

Yönlü, Ö., Karabacak, V., Altunel, E. and Akyüz, H.S. 2012. Paleoseismological slip rate on the East Anatolian Fault Zone around Türkoğlu. International Earth Science Colloquium on the Aegean Region, IESCA-2012, 1–5 October 2012, Izmir.

Yönlü, Ö., Altunel, E. and Karabacak, V. 2017. Geological and geomorphological evidence for the southwestern extension of the East Anatolian Fault Zone, Turkey. *Earth and Planetary Science Letters*, **469**, 1–14, https://doi.org/10.1016/j.epsl.2017.03.034